ACS APPLIED MATERIALS & INTERFACES

Research Article

www.acsami.org

Water-Soluble Triscyclometalated Organoiridium Complex: Phosphorescent Nanoparticle Formation, Nonlinear Optics, and Application for Cell Imaging

Yuanpeng Fan,[‡] Jingyi Zhao,[†,§] Qifan Yan,[‡] Peng R. Chen,*[,†] and Dahui Zhao*[,‡]

[‡]Beijing National Laboratory for Molecular Sciences, Department of Applied Chemistry and the Key Laboratory of Polymer Chemistry and Physics of the Ministry of Education, College of Chemistry, Peking University, Beijing 100871, China

[†]Beijing National Laboratory for Molecular Sciences, Synthetic and Functional Biomolecules Center, Department of Chemical Biology, Peking-Tsinghua Center for Life Sciences, Peking University, Beijing 100871, China

[§]Laboratory of Chemical Genomics, School of Chemical Biology and Biotechnology, Shenzhen Graduate School of Peking University, Shenzhen 518055, China

Supporting Information

ABSTRACT: Two water-soluble triscyclometalated organoiridium complexes, **1** and **2**, with polar side chains that form nanoparticles emitting bright-red phosphorescence in water were synthesized. The optimal emitting properties are related to both the triscyclometalated structure and nanoparticle-forming ability in aqueous solution. Nonlinear optical properties are also observed with the nanoparticles. Because of their proper cellular uptake in addition to high emission brightness and effective two-photon absorbing ability, cell imaging can be achieved with nanoparticles of **2** bearing quaternary ammonium side chains at ultra-low effective concentrations using NIR incident light via the multiphoton excitation phosphorescence process.

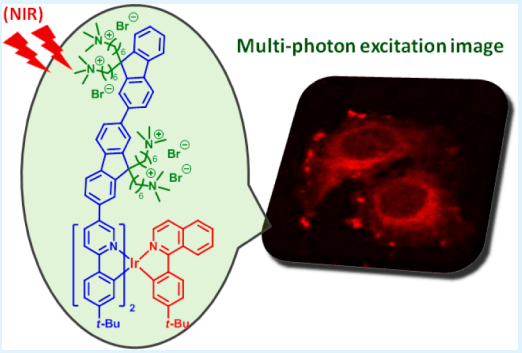

KEYWORDS: *triscyclometalated iridium, water solubility, phosphorescent nanoparticles, phosphorescence cell imaging, multiphoton excitation phosphorescence*

INTRODUCTION

A number of imaging techniques have been developed over recent decades for studying the structures and functions of biological systems.[1,2] Among them, fluorescence microscopy is of particular value for allowing dynamic, real-time visualization both in vivo and in vitro.[3−5] Carefully designed fluorescent probes and labels with properties specifically tailored for targeted functions present additional advantages of this technique. Moreover, with the advancement of nonlinear optical techniques, multiphoton excitation looms as a more potent method compared with conventional linear optical microscopy because it utilizes significantly longer-wavelength, lower-energy excitation light with greater penetration depth, reduced photodamage, less scattering, and reduced interference from cellular autofluorescence.[6−8] Organic small molecules and conjugated polyelectrolytes have both been studied as two-photon fluorescent probes for cell imaging.[9−15]

Compared with fluorophores, phosphorescent molecules possess additional advantages as optical bioprobes. With a much longer lifetime of the triplet excited state and significantly enlarged Stokes shift, phosphorescence reduces interference from excitation light, auto-fluorescence, and self-quenching more effectively. Metal complexes of lanthanides,[16−19] ruthenium,[20−26] iridium,[27−34] and platinum[35−38] have all been investigated as phosphorescent cellular probes. However, the typical low-emission quantum yields (Φ) of transition-metal complexes in water create difficulties for their application.[27,39,40] Employing higher probe concentrations to compensate for the low-emission brightness necessarily entails increased cytotoxicity. Hence, phosphorescent probes with high emission brightness in water are highly desirable and vastly pursued. Furthermore, if nonlinear optical properties are attainable, then multiphoton excitation phosphorescence (MPEP) using a longer excitation wavelength is apparently even more favorable for bioimaging. Hence, complexes with two-photon excitation phosphorescence (2PEP) have been intensely studied for bioapplications.[18,19,33,36−38]

With high phosphorescence Φ, organoiridium molecules have emerged as particularly attractive candidates for cell imaging. Thus far, biscyclometalated iridium complexes have been more widely investigated.[27−31] Triscyclometalated iridium analogues, which could potentially serve as superior phosphorescent bioprobes that have even higher emission Φ as well as better photo- and chemo-stability, are much less studied.[32−34]

Received: March 26, 2013
Accepted: February 11, 2014
Published: February 11, 2014

   dx.doi.org/10.1021/am500549y | ACS Appl. Mater. Interfaces 2014, 6, 3122−3131

Scheme 1. Synthesis of Molecules 1−3

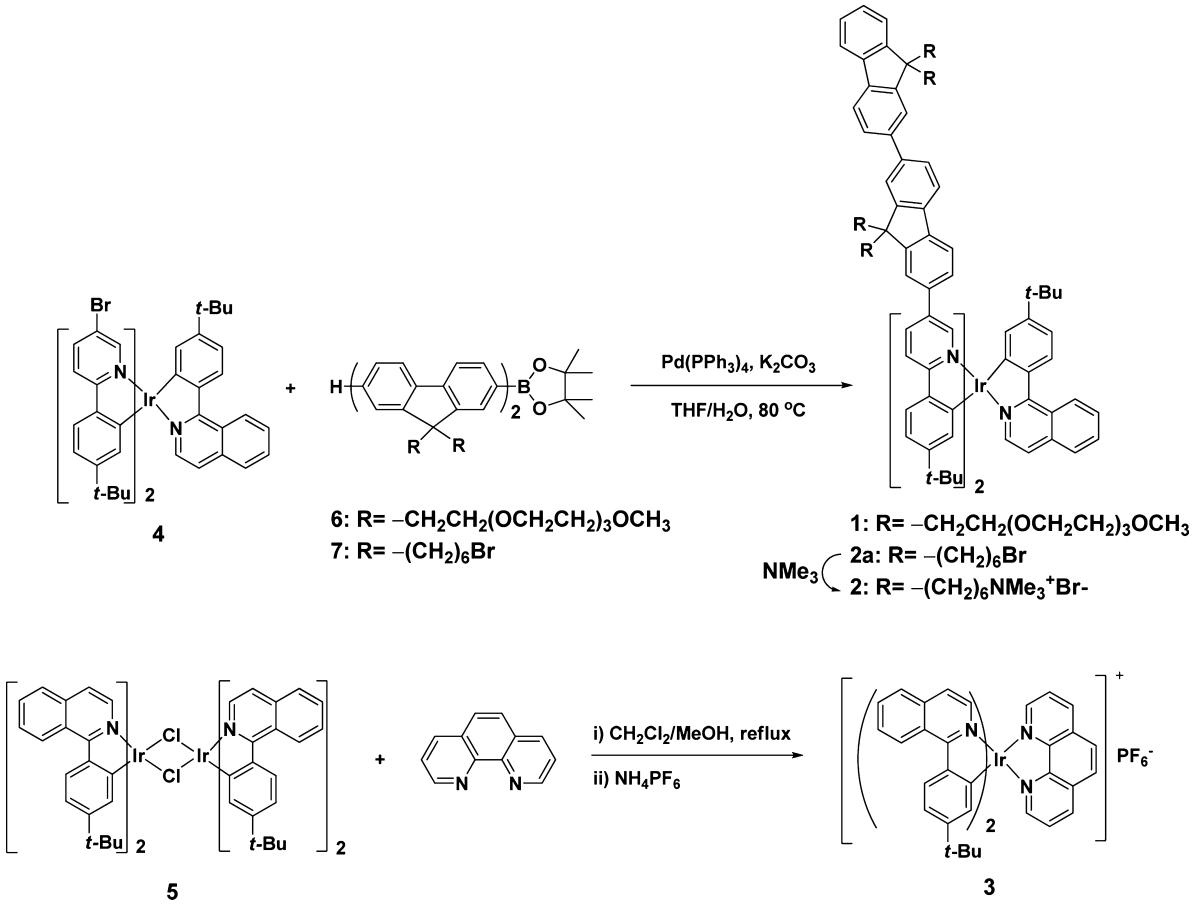

Having all ligands tethered to the metal center through robust carbon−metal bonds, triscyclometalated iridium complexes should also produce lower cytotoxicity. One of the reasons that these complexes have been less-explored for bioapplications may be that they are typically electronic-neutral molecules and thus have very limited water solubility.

In the current work, we designed two water-soluble triscyclometalated iridium complexes, **1** and **2** (Scheme 1), and studied their behaviors under aqueous conditions as well as their potential for cell imaging. With a neutral core, the water solubility of these molecules was realized by attaching polar side chains to the bisfluorenyl phenylpyridine (ppy) ligands. Two types of side chains, oligo(ethylene glycol) and a quaternary ammonium terminated alkyl group, were employed to confer water solubility. Both complexes were found to form nanoparticles in water, which emitted bright-red phosphorescence. Particularly, nanoparticles of **2** (**NP2**) with ionic ammonium side chains showed adequate cellular uptake. By virtue of the optimal-emitting ability of the particle, cellular imaging was performed at submicromolar effective concentrations. Experimental results also demonstrated that **NP2** outperformed biscyclometalated ionic reference compound **3** in both effective imaging concentration limit and cell viability. Furthermore, as **NP2** manifested a perceptible 2PEP property, cell imaging was accomplishable with near-infra-red (NIR) incident light ranging from 680 to 800 nm, also at very low probe concentrations. Three-photon excitation phosphorescence (3PEP) was also detected for **NP2** at 800 nm by photophysical characterizations.

RESULTS AND DISCUSSION

Synthesis and Photophysical Characterization. Complexes **1** and **2** were prepared via Suzuki coupling between bromine-substituted triscyclometalated $Ir(ppy)_2(piq)$ (piq = phenylisoquinoline) and corresponding bisfluorenyl boronates (Scheme 1 and Supporting Information).[41,42] Two different types of side chains were appended to the 9-position of fluorene units. Complex **1** incorporated tetraethylene glycol monomethyl ether[43] side chains, and analogue **2** featured quaternary ammonium salt terminated alkyl groups,[44,45] both of which bestowed evident water solubility to the complexes. Biscyclometalated ionic complex **3** was also synthesized,[46] serving as a reference molecule for comparison study. The structures of **1**−**3** were characterized and confirmed by ^1H and ^{13}C NMR in addition to mass spectroscopy.

We first studied the linear optical properties of **1** and **2** in methanol. UV−vis absorption spectra were recorded at 10 μM (Figure 1 and Table 1). The major absorption peaks emerged at 350−360 nm for both complexes, which were assigned to the spin-allowed ligand-centered (LC) $\pi-\pi^*$ transition of the bifluorenyl ppy ligands.[41,42] Minor absorption bands appearing at over 400 nm were attributed to the metal-to-ligand charge-transfer (MLCT) transitions. In comparison, biscyclometalated **3** exhibited a much weaker absorption band because of the absence of conjugated bisfluorenyl groups. Complexes **1** and **2** emitted red phosphorescence around 635 nm in degassed methanol, typical for the ^{3}MLCT emission of triscyclometalated iridium complexes bearing piq ligand. In the same solvent, complex **3** emitted phosphorescence at 595 nm.[46] The

dx.doi.org/10.1021/am500549y | ACS Appl. Mater. Interfaces 2014, 6, 3122−3131

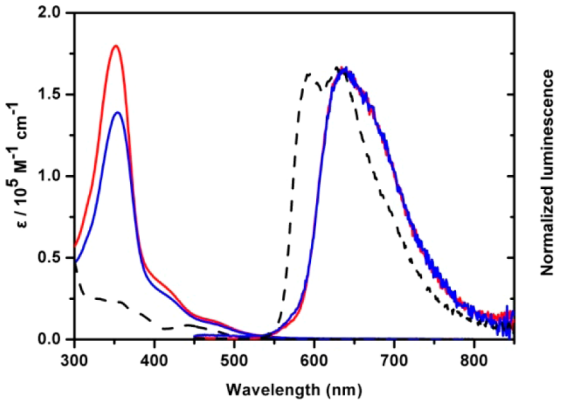

Figure 1. Absorption and emission spectra of **1** (red), **2** (blue), and **3** (black dashed) in methanol (absorption was recorded at 10 μM; emission was collected from degassed solutions excited at their respective absorption maxima with an OD of 0.1).

phosphorescence quantum yields were found to be around 0.4 for both **1** and **2** in methanol solution, which were also comparable to that of **3** (Table 1). Very similar phosphorescence lifetimes of less than 2 μs were measured for **1** and **2** in methanol. Because the absorption and emission spectra were almost identical for **1** and **2** in methanol, this suggests that the side-chain structures had little effect on the optical properties of these complexes in the single-molecule state.[47]

Intermolecular Aggregation and Nanoparticle Properties. Because of their amphiphilic structures (neutral complexes with hydrophobic hydrocarbon ligands and hydrophilic polar side chains), both **1** and **2** were found to aggregate intermolecularly in water, but their behaviors appeared to differ slightly. Directly dispersing a concentrated THF solution of **1** into water with stirring resulted in a cloudy suspension of large particles (several hundred nanometers in diameter). Nonetheless, when a concentrated THF solution of **1** was injected into a mixture of H_2O and THF and the organic solvent was subsequently removed by continuously bubbling through nitrogen gas, smaller nanoparticles of **1** (**NP1**) of relatively uniform size were obtained.[48] The mean hydrodynamic diameter of the thus obtained particles was approximately 80 nm, as revealed by dynamic light scattering (DLS, Figure S3). When a similar procedure was conducted for **2** using methanol as the co-solvent with water, NPs of similar sizes were also observed. Actually, because the solubility of complex **2** was noticeably higher than that of **1** in water, a special procedure for treating a mixed solvent was not necessary for **2**. NPs with relatively uniform size could be attained by directly dispersing a highly concentrated methanol solution of **2** into a large amount of water. Figure 2 shows the hydrodynamic radius distribution

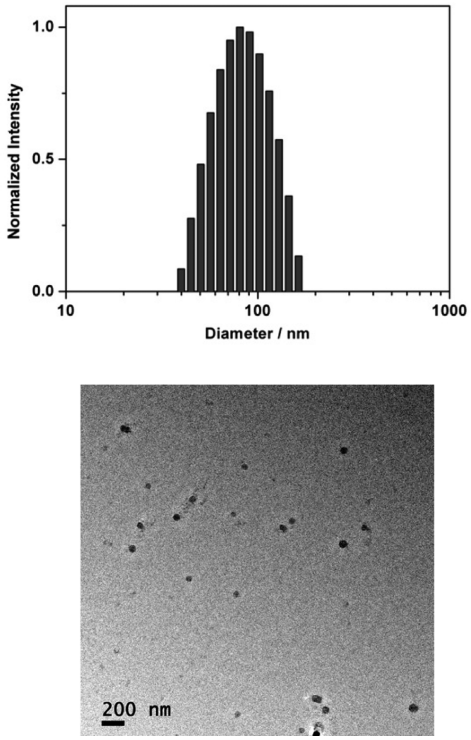

Figure 2. Hydrodynamic radius distribution (effective concentration: 1 μM in H_2O) and TEM image of **NP2**.

of **NP2** at an effective concentration of 1 μM. Such a facile NP preparation procedure allowed **NP2** to be conveniently applied for cell imaging (vide infra). However, no DLS signal was detected for an aqueous solution of **3**, indicating that this molecule was molecularly dissolved in water without evident aggregation.

Transmission electron microscopy (TEM) and atomic force microscopy (AFM) further confirmed the NP formation by **1** and **2**. On the basis of the statistical analyses performed on the TEM images, **NP2** had an average diameter of ca. 56 nm (Figure 2). A smaller particle size was given by TEM than DLS, likely because of the shrinkage of hydrated NPs during TEM sample preparation.[49,50] AFM also corroborated the nanoscale

Table 1. Absorption and Photoluminescence Properties of Compounds 1−3

		absorption		photoluminescence			
compound	solvent	λ_{abs} (nm)[a]	ε (10^5 M^{-1} cm^{-1})	λ_{em} (nm)[a]	τ (μs)[b]	Φ_p[c]	$\varepsilon_{350} \times \Phi_p$ (10^5 M^{-1} cm^{-1})[d]
1	MeOH	352	1.79	634	1.6	0.45	0.81
NP1	H_2O	361	1.40	629	0.6	0.13	0.18
2	MeOH	353	1.39	635	1.7	0.36	0.50
NP2	H_2O	355	1.23	632	1.1	0.13	0.16
3	MeOH	358	0.22	592, 628	4.3	0.41	0.09
	H_2O	359	0.23	595, 632	0.9	0.023	0.005

[a]Absorption and emission maxima. [b]Lifetimes were measured by time-correlated single-photon counting using NanoLED (339 or 369 nm) as the excitation light source. [c]$Ir(piq)_3$ (Φ_p = 0.6 in CH_2Cl_2) was used as the standard for the phosphorescence quantum yield measurement. [d](Apparent) phosphorescence quantum yield (Φ_p) multiplied by (apparent) molar extinction coefficient (ε) at the excitation wavelength (350 nm) was used as an index of emission brightness.

sizes of the particles (Figure S4),[51] which are suitable for cellular uptake.[52−54]

Photophysical properties of these NPs were then compared with those of single molecules.[47] The absorption spectra of **NP1** and **NP2** in water were both red-shifted compared to those in methanol. The reason for such red shifting was attributed to the more planariz bifluorenyl ppy ligands in the aggregated state. The attenuated apparent extinction coefficients of **1** and **2** in water also corroborated the aggregate formation (Table 1). Furthermore, **NP1** showed progressively red-shifted absorption at increased effective concentrations in water (Figure S2), suggesting continuously condensed molecular packing. The absorption wavelength of **NP2** in water was, however, nearly concentration-independent, implying that more compact molecular packing did not happen to **2** at higher concentrations. This likely resulted from the electrostatic repulsion among the charged ammonium side chains. Similar phenomena were also observed with polyelectrolyte aggregates.[55] Nearly identical absorption spectra were collected for **3** from methanol and aqueous solutions, consistent with the notion that no intermolecular aggregation occurred for this molecule in water.

Remarkably, both **NP1** and **NP2** manifested bright-red phosphorescence under aqueous conditions. The apparent phosphorescence quantum yields, Φ_p, in water were determined to be about 0.13 for both NPs, whereas the Φ_p of **3** was only 0.023 in water. To the best of our knowledge, the apparent Φ_p values of **NP1** and **NP2** are among the highest values of all red-emitting metal complexes in water. Combined with their good absorbing properties, the emission brightness (indexed by the apparent values of $\varepsilon \times \Phi$) of **NP1** and **NP2** was roughly 30 times that of **3** (Figure S1). However, it should be noted that the phosphorescence Φ_p values of **1** and **2** were actually very similar to that of **3** in methanol (all around 0.4, Table 1). In other words, when the solvent was switched from methanol to water, the emissions of **NP1** and **NP2** were less quenched compared to that of **3**. It was thus suggested that NP formation helped to maintain a high emission efficiency in aqueous solution. Water molecules are well-known to quench low-energy triplet emissions via vibrational coupling.[27,39,40] Therefore, phosphorescent molecules typically have very low Φ_p in water. Such a strong emission-quenching effect was also demonstrated by **3** in the current study. Presumably by forming NPs, the emissive moieties of **1** and **2** were concealed inside particles, whereas the hydrophilic side chains were positioned at the periphery and effectively shielded the particle core from water molecules. Thereby, solvent-induced quenching was greatly inhibited, facilitating the high emitting efficiencies of the NPs.

This hypothesis of NP formation repressing the solvent-quenching effect was further substantiated by time-resolved photophysical data. The phosphorescence lifetimes of **1** and **2** were reduced only moderately when the solvent was changed from methanol to water, whereas the emission lifetime of **3** was shortened to a greater extent under the same conditions. The less-curtailed lifetimes of **NP1** and **NP2** further prove that the excited states of molecules in the NPs were less influenced by water compared to molecularly dispersed **3**. The emission-wavelength changes provided additional evidence for the shielding effect in NPs. Upon the solvent switch from methanol to water, the emission band of **3** was slightly red-shifted. Such red shifting is typical for molecules having an excited state of charge-transfer characteristics because polar solvents such as water better stabilize the more-polar excited state. In contrast, the emission spectra of **NP1** and **NP2** were blue-shifted when experiencing the same solvent change. This unusual shifting trend could also be explained by aggregate formation. Presumably, inside the particles, aggregated molecules created a less-polar local environment compared to those in methanol and water, causing the blue shifting in the emission. Furthermore, **NP1** manifested an even shorter emission wavelength compared to **NP2**, indicating an even less-polar local environment in the former than the latter. This is consistent with the previous conclusion that the ethylene glycol side chains induced more compact molecular packing. The charged ammonium side chains might also have been the reason for the slightly higher local polarity in **NP2**. The solvent molecules should nonetheless be effectively excluded in both, as suggested by the similar apparent emission Φ_p.

Cell Imaging. Because the high emission brightness of **NP1** and **NP2** in water is favorable for cell imaging, these complexes were subsequently tested for such a purpose. Decent cellular uptake was shown by **NP2** and **3**, but a less-optimal result was observed for **NP1** (Figure S6). One of the reasons for the relatively poor uptake of **NP1** was speculated to relate to the particle size. As mentioned above, a special procedure involving gradual removal of the organic component from a binary solvent was required for **1** to form NPs, but such a process was not compatible with cell incubation. Directly dispersing this complex into the cell culture resulted in much larger particles of irregular sizes. Previous literature also reported inferior cell uptake of ethylene glycol chains compared to quaternary ammonium structures because of evidently prohibited immunogenicity and nonspecific cellular uptake.[56] Therefore, subsequent cell imaging study was focused on **NP2**.

Cells were incubated with **NP2** for 6 h prior to the imaging experiments. Figure 3 shows the images of HeLa cells treated

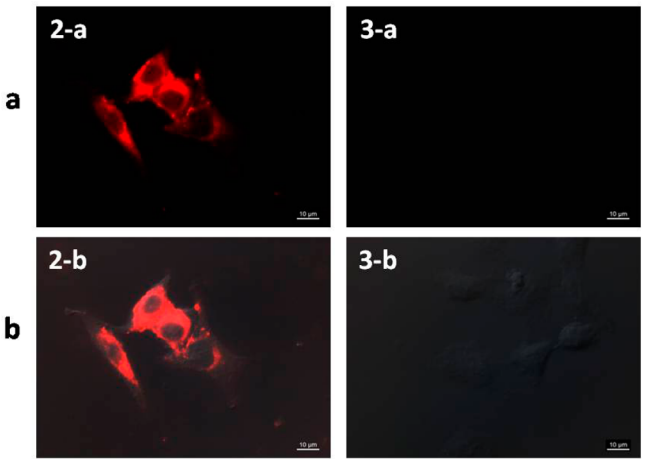

Figure 3. Images of HeLa cells upon incubation with **NP2** (left) or **3** (right) for 6 h, both at 0.5 μM: (a) phosphorescence images (excited at 405 nm) and (b) overlay with bright-field images (scale bars, 10 μm; exposure time, 19 ms).

with **NP2** at an effective concentration of 0.5 μM and illuminated by UV light. Clearly, the dye was taken by the cytoplasm but not the nuclei. In comparison, cells treated with **3** under the same conditions are also shown. At such a low concentration, **NP2** still generated intense intracellular red phosphorescence, affording decent imaging results, whereas cells containing **3** were nearly invisible with the same exposure

time. When the concentration was increased to 1 μM, cells incubated with **3** also exhibited phosphorescence, but only at a much lower emission intensity than **NP2** (Figure S9). It was further demonstrated that proper imaging could still be achieved with **NP2** even when the incubation concentration was lowered to 0.2 μM (Figure S8). Such a concentration was nearly an order of magnitude lower than the typical loading of phosphorescent dyes reported in the literature. To prove the cellular uptake of **NP2** further, we also acquired images with the microscope scanning along the *z* axis, which unambiguously depicted that the red-emitting dyes were located in the cells (Figure 4).

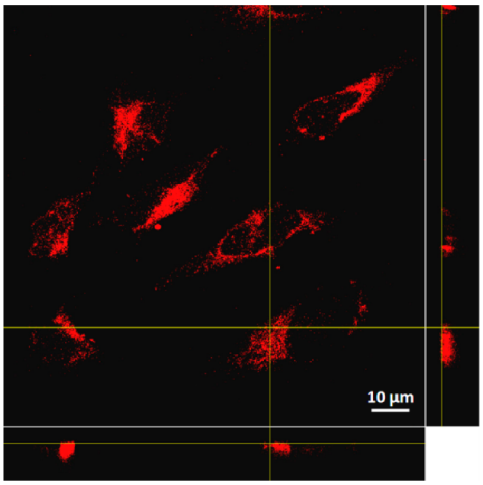

Figure 4. Luminescence images (including *z*-axis scanning) of HeLa cells incubated with **NP2** for 6 h at 0.5 μM (excited at 405 nm).

Subsequent phosphorescence lifetime measurements (PLIM) showed an intracellular luminescence lifetime range of 0.7−1.0 μs (Figure S10). Single-point lifetimes measured in different regions of the cytoplasm gave a similar average value of ca. 0.8 μs (Figure S11). These measurements offered relatively consistent lifetimes, but these values were slightly longer than that detected for **NP2** in aerated water (τ = 0.6 μs).[57] The following experiment helped to explain the origin of such a difference. When bovine serum albumin was added to a solution of **NP2** in PBS, the lifetime of **NP2** was observed to increase from 0.6 to 0.9 μs (Figure S12). At the same time, the emission intensity was enhanced perceptibly. These results suggested that **NP2** was likely bound to hydrophobic organelles in the cytoplasm.[58]

Subsequently, the potential of **NP2** serving as an MPEP imaging probe was investigated by conducting imaging with a NIR light source. It was found that proper imaging could be achieved with an excitation wavelength ranging from 680 to 800 nm and emission signals collected in the red visible range of 570 to 640 nm. At the excitation wavelength of 690 nm, the incubation concentration could be lowered to 0.5 μM, which still afforded desirable imaging results. When a much longer excitation wavelength (e.g., 800 nm) was applied, a slightly higher incubation concentration was necessary, which was still no more than 3 μM (Figure 5). As a control experiment, no MPEP image was observable for **3** under the same conditions.

The photostability of **NP2** was examined under the same conditions for cell imaging. With HeLa cells incubated with **NP2** being exposed to a UV light of 405 nm, the luminescence intensity change was monitored for 20 min (Figure S13). Negligible photobleaching was observed during this period of time, indicating sufficient photostability. Quantitative experiments showed that the photodecomposition quantum yields[59] of **NP2** were about 1.2×10^{-5} and 9×10^{-6} in deaerated aqueous solution upon excitation at 405 and 800 nm, respectively. These results demonstrate the suitability of **NP2** for bioimaging applications.

Nonlinear Optical Properties. To prove the MPEP imaging results further, we then conducted nonlinear optical characterization for **NP2** in aqueous solution. To match the microsecond-scale excited-state lifetime of **NP2**, a low-repetition rate (1 kHz) laser was employed to characterize its MPEP properties. When the excitation power density was set in the range of 10 to 10^2 GW cm^{-2}, 2PEP ability was demonstrated by **NP2** in aqueous solution, as evidenced by

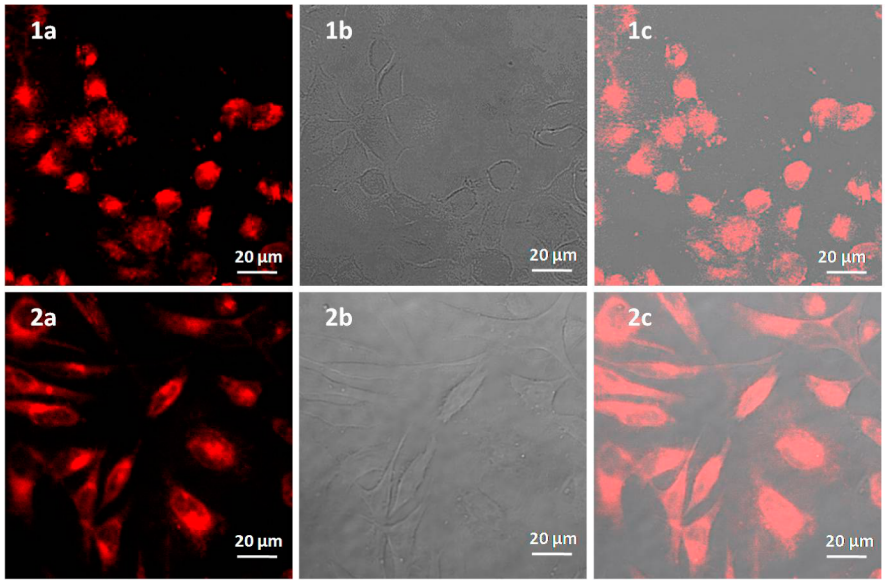

Figure 5. Images of HeLa cells upon incubation with **NP2** for 6 h: (a) phosphorescence images, (b) bright-field images, and (c) overlaid images (top: excited with 800 nm light, incubation concentration = 3 μM; bottom: excited with 690 nm light, incubation concentration = 0.5 μM).

the magnitude of emission intensity change with the excitation power (Figure 6). Namely, the log−log plot of phosphorescence intensity as a function of excitation power showed a linear correlation with a slope of ca. 2. Accordingly, an apparent two-photon absorption (2PA) cross-section of 33 GM was determined. Such 2PEP properties of **NP2** further validated its cell imaging capability using a NIR excitation source.

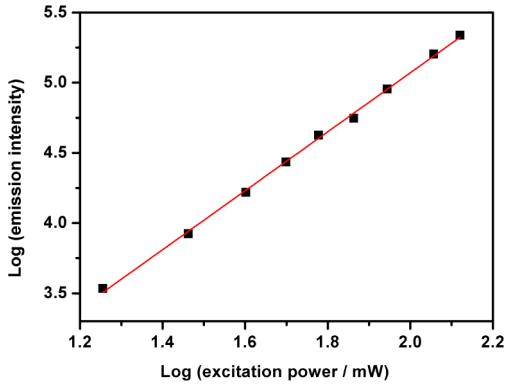

Figure 6. Log−log plot of emission intensity of **NP2** against the excitation power density (800 nm, 1 kHz) in degassed water at an effective concentration of 10^{-4} M (slope = 2.1, r^2 = 0.998, power density of 10 to 10^2 GW cm^{-2}).

Notably, when a much higher excitation power density (~10^3 GW cm^{-2}) was applied to a **NP2** solution at the same wavelength, the log−log plot of emission intensity versus excitation power revealed a linear dependence with a slope of roughly 3 (Figure S16), suggesting the occurrence of a three-photon excitation phosphorescence (3PEP) process under such high-power-density conditions. It was thus proposed that **NP2** possessed both two- and three-photon-absorbing abilities at 800 nm.[60−65] On the basis of the 3PEP intensity, **NP2** was estimated to have an attractive 3PA ability for water-soluble systems.[6,63,64] Nonetheless, it should be noted that the cell imaging results using the NIR light source were more likely realized via a 2PA rather than a 3PA process because 3PEP was observable only at very high excitation power, and the excitation power density applied in the fluorescence microscope was merely ~10 GW cm^{-2}.

Additionally, at wavelengths shorter than 800 nm, a 2PA process probably dominated, and a 3PA cross-section should reduce significantly with decreased wavelength. However, because the low-repetition-frequency laser was available only at 800 nm, subsequent investigation on the 2PEP properties of **NP2** at shorter excitation wavelengths were conducted using a high-repetition-rate (83 MHz) laser. At a constant excitation power, the emission intensity was observed to grow as the excitation wavelength was changed from 800 to 720 nm (Figure S14), suggesting that higher 2PEP capacity was available in this range. Because of the mismatching of the temporal distance among laser pulses (83 MHz) with the excited-state lifetime, 2PA cross sections at wavelengths other than 800 nm could not be precisely measured for **NP2**, but the experimentally observed emission intensity change with excitation power at least confirmed the nonlinear nature of the absorption in this range (Figure S15). This conclusion was also corroborated by the fact that no linear absorption was observed for **NP2** in water beyond 600 nm.

MTT Assay. Cellular toxicity of **NP2** was then investigated by the MTT assay. In vitro viability of HeLa cells was examined by incubation with **NP2** or **3** at a concentration of 1 μM for given periods of time, ranging from 6 to 72 h. The viability percentage of treated cells was calibrated relative to that of untreated cells. The viability of the latter was defined as 100% (Figure 7). The results showed that the viability of cells incubated with **NP2** stabilized at a value slightly less than 80% after 24 h, whereas the viability of cells treated with **3** continued to drop over the entire monitored time, and only less than 15% of the cells were still alive after 72 h. The observed lower toxicity of **NP2** was likely related to two factors. First, all three ligands in **2** were connected to the iridium center via robust carbon−metal bonds, which greatly stabilized the molecular structure. Additionally, the NP formation might also be responsible for the lower cytotoxicity.[66,67]

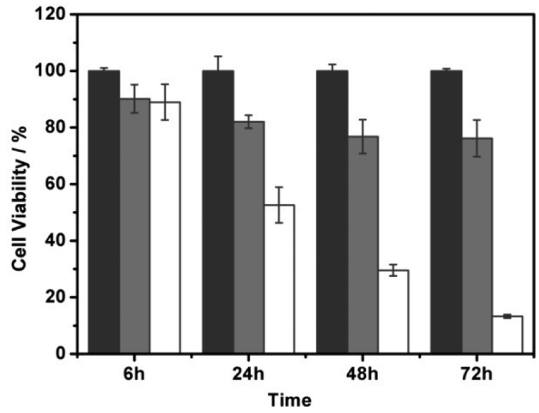

Figure 7. In vitro cell viability data of HeLa cells upon incubation with **NP2** (gray) and **3** (white) at 1 μM for the indicated periods of time at 37 °C (the viability of untreated cells was defined as 100%, dark gray).

CONCLUSIONS

Two water-soluble triscyclometalated iridium complexes were synthesized. The neutral complex backbones decorated with polar side chains conferred adequate water solubility. Both molecules were found to form NPs emitting bright-red phosphorescence in water. The relatively high emitting efficiencies in H_2O (apparent Φ = 0.13) were facilitated by both the triscyclometalated structure and NP forming process, the latter of which effectively inhibited the solvent-induced phosphorescence quenching. Proper cellular uptake was observed for **NP2** bearing quaternary ammonium side chains. By virtue of the high emission brightness of **NP2**, cell imaging could be performed at submicromolar effective dye concentrations. Furthermore, photophyscial studies demonstrated nonlinear absorption abilities of **NP2**, with a 2PA cross-section of 33 GM determined at 800 nm in water. 3PEP behavior was also detected at higher excitation power. Impressively, with the highly efficient emitting ability exhibited by **NP2** in combination with a moderate 2PA cross section, desirable MPEP cell imaging results were achieved using low-energy NIR-excitation light (680−800 nm) at micromolar effective dye concentrations. The cytotoxicity and photostability of **NP2** were also characterized and shown to be suitable for bioapplications.

EXPERIMENTAL SECTION

Materials and Instruments. All chemicals were used as received unless otherwise indicated. NMR spectra were recorded on Varian Mercury plus 300, Bruker AVANCE III 400, or Bruker AVANCE III 500. ESI-TOF mass spectra were recorded on a Bruker Apex IV FTMS mass spectrometer. UV−vis absorption spectra were recorded on a Hitachi U-4100 spectrophotometer. Photoluminescence spectra were recorded on a Horiba Jobin Yvon FluoroMax-4P spectrofluorometer. Lifetime measurements were performed by time-correlated single-photon counting using a Horiba Jobin Yvon FluoroHub-B instrument, with a NanoLED of 370 nm as the excitation source. Dynamic light-scattering (DLS) measurements were carried out using ALV-5000/E/WIN multiple tau digital correlator with a Spectra-Physics 2017 22 mW Ar laser at 632.8 nm. TEM images were acquired with a Tecnai F20 transmission electron microscopy operating at 200 kV.

Synthesis and Characterization. ***1***. A Schlenk tube containing **4** (11 mg, 0.010 mmol), **6** (29 mg, 0.022 mmol), potassium carbonate (0.14 g, 1.0 mmol), and $Pd(PPh_3)_4$ (1.0 mg, 0.86 μmol) was evacuated and backfilled with nitrogen three times. Degassed THF (0.5 mL) and H_2O (0.5 mL) were added to the tube via a syringe. The mixture was stirred at 80 °C for 40 h. After being cooled to room temperature, the mixture was extracted with ethyl acetate. The organic phase was washed with brine and then dried over anhydrous Na_2SO_4. After the solvent was removed under reduced pressure, the crude product was purified by flash column chromatography and eluted with CH_2Cl_2/MeOH (50:1, v/v) to give **1** as a red solid (10 mg, 31%). ^{1}H NMR ($CDCl_3$, 300 MHz, ppm): δ 9.10 (m,1H), 8.20 (d, 1H, J = 8.4 Hz), 8.07−7.90 (m, 6H), 7.80−7.59 (m, 23H), 7.49−7.32 (m, 10H), 7.10 (m, 2H), 6.97 (m, 2H), 6.87 (d, 1H, J = 1.8 Hz), 6.70 (s, 1H), 3.52−3.12 (m, 120H), 2.89−2.45 (m, 32H), 1.21 (s, 9H), 1.15 (s, 9H), 1.11 (s, 9H). ^{13}C NMR (100 MHz, $CDCl_3$, ppm): δ 167.9, 166.1, 165.6, 165.2, 164.7, 162.2, 160.9, 152.2, 152.1, 152.0, 150.3, 149.9, 149.8, 149.7, 149.1, 145.1, 144.9, 142.6, 140.9, 140.5, 140.3, 140.0, 139.9, 138.9, 136.8, 136.7, 136.0, 135.2, 134.9, 134.5, 133.9, 133.7, 130.2, 129.7, 128.2, 127.6, 127.5, 126.7, 126.3, 125.6, 123.4, 123.1, 1221.6, 121.4, 120.5, 120.3, 120.1, 119.6, 118.2, 117.1, 116.9, 111.3, 71.8, 70.6, 70.5, 70.1, 69.9, 66.9, 66.8, 59.0, 58.9, 51.4, 51.0, 39.8, 39.6, 34.4, 34.3, 31.4, 31.2. ESI-TOF MS (m/z): $[M + H]^+$ calcd for $C_{173}H_{226}IrN_3O_{32}$, 3051.9; found, 3052.1. ESI-TOF HRMS (m/z): $[M + 3Na]^{3+}$ calcd, 1040.1834; found, 1040.1836.

2a. A Schlenk tube containing **4** (18 mg, 0.017 mmol), **7** (36 mg, 0.034 mmol), potassium carbonate (0.14 g, 1.0 mmol), and $Pd(PPh_3)_4$ (2.0 mg, 1.7 μmol) was evacuated and backfilled with nitrogen three times. Degassed THF (2 mL) and H_2O (0.5 mL) were added to the tube via a syringe. The mixture was stirred at 80 °C for 23 h. After being cooled to room temperature, the mixture was extracted with ethyl acetate. The organic phase was washed with brine and then dried over anhydrous Na_2SO_4. After the solvent was removed under reduced pressure, the crude product was purified by flash column chromatography and eluted with petroleum ether/CH_2Cl_2 (10:1, v/v) to give **2a** as a red solid (17 mg, 36%). ^{1}H NMR ($CDCl_3$, 300 MHz, ppm): δ 9.06 (d, 1H, J = 8.4 Hz), 8.18 (d, 1H, J = 8.4 Hz), 8.06−7.53 (m, 29H), 7.40−7.27 (m, 10H), 7.12−6.96 (m, 4H), 6.80−6.78 (m, 2H), 3.29−3.10 (m, 16H), 2.06−1.56 (m, 32H), 1.32−0.54 (m, 75H). ^{13}C NMR (100 MHz, $CDCl_3$, ppm): δ 167.0, 166.1, 165.4, 165.2, 164.5, 162.1, 160.9, 152.6, 152.1, 152.0, 150.9, 149.7, 149.3, 147.2, 144.9, 142.4, 140.7, 140.5, 140.3, 140.0, 139.7, 138.9, 136.8, 136.7, 136.3, 135.2, 134.9, 134.6, 133.8, 133.4, 130.1, 128.2, 127.6, 127.5, 126.6, 126.3, 125.6, 123.4, 123.2, 121.6, 121.4, 120.5, 120.4, 120.1, 119.6, 118.2, 117.2, 116.9, 111.3, 60.2, 55.9, 55.6, 55.3 40.4, 40.1, 34.6, 34.4, 32.9, 32.1, 31.4, 31.3, 29.9, 29.1, 27.8, 23.7. ESI-TOF MS (m/z): $[M + H]^+$ calcd for $C_{149}H_{170}Br_8IrN_3$, 2834.6524; found, 2834.6520.

2. **2a** (17 mg, 0.006 mmol) was dissolved in THF (4 mL). After the solution was cooled to −78 °C, an ethanol solution of trimethylamine (1.5 mL) was added. The mixture was stirred at room temperature for 24 h. Then, H_2O (2 mL) was added to the mixture, and **2** was precipitated as a red solid (17 mg, 83%). ^{1}H NMR (CD_3OD, 300 MHz, ppm): δ 9.05 (m, 1H), 8.23−7.74 (m, 30H), 7.57−7.35 (br, 10H), 7.15−6.88 (m, 6H), 3.40−3.24 (m, 16H), 3.04 (s, 72H), 2.25−1.90 (br, 16H), 1.70−1.43 (br, 16H), 1.29−0.88 (m, 59H), 0.88−0.46 (br, 16H). ^{13}C NMR (125 MHz, DMSO-d_6, ppm): δ 165.1, 164.7, 160.0, 151.7, 151.6, 151.2, 151.1, 150.9, 150.3, 150.2, 143.9, 143.8, 141.9, 140.6, 140.4, 140.3, 140.1, 139.6, 139.4, 139.0, 136.4, 136.1, 134.5, 134.4, 133.9, 133.4, 130.9, 129.5, 128.6, 127.8, 127.3, 127.2, 127.0, 126.8, 125.9, 125.7, 125.5, 124.1, 122.9, 121.0, 120.7, 116.8, 110.7, 108.4, 107.9, 65.0, 64.9, 60.4, 54.8, 54.7, 52.0, 51.6, 51.5, 40.1, 40.0, 39.8, 39.7, 39.6, 39.5, 39.2, 39.0, 38.8, 34.1, 33.9, 31.2, 31.1, 30.9, 28.9, 28.6, 28.5, 25.3, 25.0, 23.3, 23.2, 22.0, 21.9. ESI-TOF HRMS (m/z): $[M - 3Br]^{3+}$ calcd for $C_{173}H_{242}Br_8IrN_{11}$, 1022.1604; found, 1022.1618.

3. To a mixture of CH_2Cl_2 and methanol (30 mL, 2:1 v/v) were added 1,10-phenanthroline (40 mg, 0.20 mmol) and **5** (0.15 g, 0.10 mmol) under a N_2 atmosphere. The reaction mixture was refluxed for 4 h. After being cooled to room temperature, KPF_6 (0.37 g, 2 mmol) was added, and the mixture was stirred for another 1 h. The solvent was then removed, and the residue was redissolved in CH_2Cl_2 (20 mL). The precipitate was filtered off, and methanol (20 ml) was layered on top of the filtrate. Red crystals of **3** (115 mg, 55%) were then formed. ^{1}H NMR ($CDCl_3$, 300 MHz, ppm): δ 8.90 (m, 2H), 8.68 (dd, 2H, J = 8.4, 1.5 Hz), 8.25 (s, 2H), 8.16 (d, 2H, J = 8.7 Hz), 8.40 (dd, 2H, J = 5.1, 1.5 Hz), 7.86−7.78 (m, 4H), 7.75−7.70 (m, 4H), 4.23 (d, 2H, J = 6.8 Hz), 7.18−7.14 (m, 4H), 6.27 (d, 2H, J = 1.8 Hz), 0.95 (s, 18H). ^{13}C NMR (100 MHz, DMSO-d_6, ppm): δ 168.4, 152.9, 152.8. 150.4, 146.2, 142.7, 140.7, 138.7, 136.4, 131.8, 131.2, 130.0, 129.0, 128.3, 127.8, 127.3, 126.9, 126.2, 125.4, 121.3, 119.3, 33.9, 30.4. ESI-TOF HRMS (m/z): $[M - PF_6]^+$ calcd for $C_{50}H_{44}F_6IrN_4P$, 893.3195; found, 893.3120.

Cell Culture and Imaging. HeLa cells were cultured in DMEM supplemented with 10% FBS and 1% pen−strep in a humidified atmosphere with 5% CO_2 at 37 °C. Cells were passaged every 2 to 3 days. For linear excitation and MPEP imaging, 2.5×10^4 per well of HeLa cells were seeded in 24-well plates containing 12 mm coverslips. Twenty-four hours later, the medium was changed to DMEM without FBS and pen−strep. Different concentrations of dyes were added into the medium, and the cells were incubated for another 6 h before being washed with cold PBS three times. The cells were fixed in 4% paraformaldehyde for 10 min at room temperature and then washed with cold PBS three times. Coverslips were mounted onto glass slides with glycerol and sealed with nail polish.

One-photon excitation images were acquired with Lecia DMI4000B inverted microscope with a DFC420C camera (excitation wavelength: 405 nm). z-axis scan images and photostability data were acquired with a Nikon A1R-si laser scanning confocal microscope (excitation wavelength: 405 nm). For PLIM, time-correlated single-photon counting measurements were performed using a HORIBA Scientific DynaMyc equipped with a Lumenera Infinity 3-1 CCD camera to collect images using a 375 nm excitation light, with emission selected via a beam splitter or filter cube. A DeltaDiode pulsed laser (Horiba; 375 nm) was used for excitation, and the emission was monitored with 514LP filter using a TBX-04 picosecond detection module. The MPEP images were acquired with FV1000MPE upright microscope with femtosecond mode-locked Ti−sapphire as the laser source (Chameleon Ultra II; repetition rate: 83 MHz) at a wavelength of 690 or 800 nm.

MTT Assay. HeLa cells (5000 cells per well) were seeded in 96-well plates. After 24 h, the cells were incubated in serum- and antibiotic-free medium with different concentrations of dyes for 6, 24, 48, or 72 h at 37 °C. Untreated cells were used as negative control. After the dye treatment, 20 μL of MTT (5 mg/mL in PBS) solutions were added into the medium, and the cells were incubated for another 4 h at 37 °C. The medium was then removed, and 200 μL of DMSO was added to each well. The plates were shaken gently for 10 min at room temperature, and the absorbance of each well was measured at 570 nm.

■ ASSOCIATED CONTENT

Supporting Information

Additional synthetic procedures and characterization data; absorption and emission spectra of **NP**, **NP2**, and **3** in water; absorption spectra of **NP1** and **NP2** in water at different concentrations; hydrodynamic radius distributions of **NP1** and **NP2** in water; tapping-mode AFM images of **NP1** and **NP2**; zeta potentials of **NP1** and **NP2**; linear excitation phosphorescence images of HeLa cells upon incubation with **NP1**, **NP2** and **3**; phosphorescence lifetime images of the HeLa cells incubated with **NP2**; phosphorescence decays of **2** and **NP2**; phosphorescence decays of **NP2** in the absence or presence of BSA in aerated PBS; luminescence decay curve of **NP2** from incubated HeLa cells; MPEP emission spectra of **NP2**; and log−log plot of emission intensity against excitation power density for **NP2**. This material is available free of charge via the Internet at http://pubs.acs.org.

■ AUTHOR INFORMATION

Corresponding Authors

*E-mail: pengchen@pku.edu.cn (P.R.C.).
*E-mail: dhzhao@pku.edu.cn (D.Z.).

Notes

The authors declare no competing financial interest.

■ ACKNOWLEDGMENTS

This work was supported by the National Natural Science Foundation of China (project nos. 51073002, 21174004, and 21222403).

■ REFERENCES

(1) Weissleder, R. Molecular Imaging in Cancer. *Science* **2006**, *312*, 1168−1171.
(2) McRae, R.; Bagchi, P.; Sumalekshmy, S.; Fahrni, C. J. In Situ Imaging of Metals in Cells and Tissues. *Chem. Rev.* **2009**, *109*, 4780−4827.
(3) Lee, J.-S.; Vendrell, M.; Chang, Y.-T. Diversity-Oriented Optical Imaging Probe Development. *Curr. Opin. Chem. Biol.* **2011**, *15*, 760−767.
(4) van de Linde, S.; Heilemann, M.; Sauer, M. Live-Cell Super-Resolution Imaging with Synthetic Fluorophores. *Annu. Rev. Phys. Chem.* **2012**, *63*, 519−540.
(5) Ha, T.; Tinnefeld, P. Photophysics of Fluorescent Probes for Single-Molecule Biophysics and Super-Resolution Imaging. *Annu. Rev. Phys. Chem.* **2012**, *63*, 595−617.
(6) Xu, C.; Zipfel, W. R.; Shear, J. B.; Wiliams, R. M.; Webb, W. W. Multiphoton Fluorescence Excitation: New Spectral Windows for Biological Nonlinear Microscopy. *Proc. Natl. Acad. Sci. U.S.A.* **1996**, *93*, 10763−10768.
(7) He, G. S.; Tan, L. S.; Zheng, Q.; Prasad, P. N. Multiphoton Absorbing Materials: Molecular Designs, Characterizations, and Applications. *Chem. Rev.* **2008**, *108*, 1245−1330.
(8) Yao, S.; Belfield, K. D. Two-Photon Fluorescent Probes for Bioimaging. *Eur. J. Org. Chem.* **2012**, 3199−3217.
(9) Zipfel, W. R.; Williams, R. M.; Webb, W. W. Nonlinear Magic: Multiphoton Microscopy in the Biosciences. *Nat. Biotechnol.* **2003**, *21*, 1369−1377.
(10) Kim, H. M.; Cho, B. R. Two-Photon Probes for Intracellular Free Metal Ions, Acidic Vesicles, and Lipid Rafts in Live Tissues. *Acc. Chem. Res.* **2009**, *42*, 863−872.
(11) Parthasarathy, A.; Ahn, H.-Y.; Belfield, K. D.; Schanze, K. S. Two-Photon Excited Fluorescence of a Conjugated Polyelectrolyte and Its Application in Cell Imaging. *ACS Appl. Mater. Interfaces* **2010**, *2*, 2744−2748.
(12) Wang, X.; Nguyen, D. M.; Yanez, C. O.; Rodriguez, L.; Ahn, H. Y.; Bondar, M. V.; Belfield, K. D. High-Fidelity Hydrophilic Probe for Two-Photon Fluorescence Lysosomal Imaging. *J. Am. Chem. Soc.* **2010**, *132*, 12237−12239.
(13) Shen, X.; Li, L.; Wu, H.; Yao, S. Q.; Xu, Q.-H. Photosensitizer-Doped Conjugated Polymer Nanoparticles for Simultaneous Two-Photon Imaging and Two-Photon Photodynamic Therapy in Living Cells. *Nanoscale* **2011**, *3*, 5140−5146.
(14) Meulenaere, E. D.; Chen, W.; Cleuvenbergen, S. V.; Zheng, M.; Psilodimitrakopoulos, S.; Paesen, R.; Taymans, J. M.; Ameloot, M.; Vanderleyden, J.; Loza-Alvarez, P.; Duan, X.; Clays, K. Molecular Engineering of Chromophores for Combined Second-Harmonic and Two-Photon Fluorescence in Cellular Imaging. *Chem. Sci.* **2012**, *3*, 984−995.
(15) Kong, B.; Zhu, A.; Ding, C.; Zhao, X.; Li, B.; Tian, Y. Conjugated Oligoelectrolyte Harnessed Polyhedral Oligomeric Silsesquioxane as Light-Up Hybrid Nanodot for Two-Photon Fluorescence Imaging of Cellular Nucleus. *Adv. Mater.* **2012**, *24*, 5844−5848.
(16) Viguier, R. F. H.; Hulme, A. N. A Sensitized Europium Complex Generated by Micromolar Concentrations of Copper(I): Toward the Detection of Copper(I) in Biology. *J. Am. Chem. Soc.* **2006**, *128*, 11370−11371.
(17) Li, L.-L.; Wu, P.; Hwang, K.; Lu, Y. An Exceptionally Simple Strategy for DNA-Functionalized Up-Conversion Nanoparticles as Biocompatible Agents for Nanoassembly, DNA Delivery, and Imaging. *J. Am. Chem. Soc.* **2013**, *135*, 2411−2414.
(18) Lo, W.-S.; Kwok, W.-M.; Law, G.-L.; Yeung, C.-T.; Chan, C. T.-L.; Yeung, H.-L.; Chen, C.-H.; Murphy, M. B.; Wong, K.-L.; Wong, W.-T. Impressive Europium Red Emission Induced by Two-Photon Excitation for Biological Applications. *Inorg. Chem.* **2011**, *50*, 5309−5311.
(19) D'Aléo, A.; Bourdolle, A.; Brustlein, S.; Fauquier, T.; Grichine, A.; Duperray, A.; Baldeck, P. L.; Andraud, C.; Brasselet, S.; Maury, O. Ytterbium-Based Bioprobes for Near-Infrared Two-Photon Scanning Laser Microscopy Imaging. *Angew. Chem., Int. Ed.* **2012**, *51*, 6622−6625.
(20) Puckett, C. A.; Barton, J. K. Methods to Explore Cellular Uptake of Ruthenium Complexes. *J. Am. Chem. Soc.* **2007**, *129*, 46−47.
(21) O'Connor, N. A.; Stevens, N.; Samaroo, D.; Solomon, M. R.; Martí, A. A.; Dyer, J.; Vishwasrao, H.; Akins, D. L.; Kandel, E. R.; Turro, N. J. A Covalently Linked Phenanthridine−Ruthenium(II) Complex as a RNA Probe. *Chem. Commun.* **2009**, 2640−2642.
(22) Svensson, F. R.; Abrahamsson, M.; Strömberg, N.; Ewing, A. W.; Lincoln, P. Ruthenium(II) Complex Enantiomers as Cellular Probes for Diastereomeric Interactions in Confocal and Fluorescence Lifetime Imaging Microscopy. *J. Phys. Chem. Lett.* **2011**, *2*, 397−401.
(23) Bergamo, A.; Gaiddon, C.; Schellens, J. H. M.; Beijnen, J. H.; Sava, G. Approaching Tumour Therapy Beyond Platinum Drugs: Status of the Art and Perspectives of Ruthenium Drug Candidates. *J. Inorg. Biochem.* **2012**, *106*, 90−99.
(24) Pierroz, V.; Joshi, T.; Leonidova, A.; Mari, C.; Schur, J.; Ott, I.; Spiccia, L.; Ferrari, S.; Gasser, G. Molecular and Cellular Characterization of the Biological Effects of Ruthenium(II) Complexes Incorporating 2-Pyridyl-2-pyrimidine-4-carboxylic Acid. *J. Am. Chem. Soc.* **2012**, *134*, 20376−20387.
(25) Ke, H.; Wang, H.; Wong, W.-K.; Mak, N.-K.; Kwong, D. W. J.; Wong, K.-L.; Tam, H.-L. Responsive and Mitochondria-Specific Ruthenium(II) Complex for Dual in Vitro Applications: Two-Photon (Near-Infrared) Induced Imaging and Regioselective Cell Killing. *Chem. Commun.* **2010**, *46*, 6678−6680.
(26) Zhang, J.-X.; Zhou, J.-W.; Chan, C.-F.; Lau, T. C.-K.; Kwong, D. W. J.; Tam, H.-L.; Mak, N.-K.; Wong, K.-L.; Wong, W.-K. Comparative Studies of the Cellular Uptake, Subcellular Localization, and Cytotoxic and Phototoxic Antitumor Properties of Ruthenium(II)−Porphyrin Conjugates with Different Linkers. *Bioconjugate Chem.* **2012**, *23*, 1623−1638.
(27) Lau, J. S.-Y.; Lee, P.-K.; Tsang, K. H.-K.; Ng, C. H.-C.; Lam, Y.-W.; Cheng, S.-H.; Lo, K. K.-W. Luminescent Cyclometalated

Iridium(III) Polypyridine Indole Complexes-Synthesis, Photophysics, Electrochemistry, Protein-Binding Properties, Cytotoxicity, and Cellular Uptake. *Inorg. Chem.* **2009**, *48*, 708−718.
(28) Li, C.; Yu, M.; Sun, Y.; Wu, Y.; Huang, C.; Li, F. A Nonemissive Iridium(III) Complex That Specifically Lights-Up the Nuclei of Living Cells. *J. Am. Chem. Soc.* **2011**, *133*, 11231−11239.
(29) Moromizato, S.; Hisamatsu, Y.; Suzuki, T.; Matsuo, Y.; Abe, R.; Aoki, S. Design and Synthesis of a Luminescent Cyclometalated Iridium(III) Complex Having *N*,*N*-diethylamino Group That Stains Acidic Intracellular Organelles and Induces Cell Death by Photoirradiation. *Inorg. Chem.* **2012**, *51*, 12697−12706.
(30) Liu, S.; Qiao, W.; Cao, G.; Chen, Y.; Ma, Y.; Huang, Y.; Liu, X.; Xu, W.; Zhao, Q.; Huang, W. Smart Poly(*N*-isopropylacrylamide) Containing Iridium(III) Complexes as Water-Soluble Phosphorescent Probe for Sensing and Bioimaging of Homocysteine and Cysteine. *Macromol. Rapid Commun.* **2013**, *34*, 81−86.
(31) Cao, R.; Jia, J.; Ma, X.; Zhou, M.; Fei, H. Membrane Localized Iridium(III) Complex Induces Endoplasmic Reticulum Stress and Mitochondria-Mediated Apoptosis in Human Cancer Cells. *J. Med. Chem.* **2013**, *56*, 3636−3644.
(32) You, Y.; Han, Y.; Lee, Y. M.; Park, S. Y.; Nam, W.; Lippard, S. J. Phosphorescent Sensor for Robust Quantification of Copper(II) Ion. *J. Am. Chem. Soc.* **2011**, *133*, 11488−11491.
(33) Ho, C.-L.; Wong, K.-L.; Kong, H.-K.; Ho, Y.-M.; Chan, C. T.-L.; Kwok, W.-M.; Leung, K. S.-Y.; Tam, H.-L.; Lam, M. H.-W.; Ren, X.-F.; Ren, A.-M.; Feng, J.-K.; Wong, W.-Y. A Strong Two-Photon Induced Phosphorescent Golgi-Specific in Vitro Marker Based on a Heteroleptic Iridium Complex. *Chem. Commun.* **2012**, *48*, 2525−2527.
(34) Steunenberg, P.; Ruggi, A.; van den Berg, N. S.; Buckle, T.; Kuil, J.; van Leeuwen, F. W. B.; Velders, A. H. Phosphorescence Imaging of Living Cells with Amino Acid-Functionalized Tris(2-phenylpyridine)-iridium(III) Complexes. *Inorg. Chem.* **2012**, *51*, 2105−2114.
(35) Chung, C. Y.-S.; Li, S. P.-Y.; Louie, M.-W.; Lo, K. K.-W.; Yam, V. W.-W. Induced Self-Assembly and Disassembly of Water-Soluble Alkynylplatinum(II) Terpyridyl Complexes with "Switchable" Near-Infrared (NIR) Emission Modulated by Metal−Metal Interactions over Physiological pH: Demonstration of pH-Responsive NIR Luminescent Probes in Cell-Imaging Studies. *Chem. Sci.* **2013**, *4*, 2453−2462.
(36) Botchway, S. W.; Charnley, M.; Haycock, J. W.; Parker, A. W.; Rochester, D. L.; Weinstein, J. A.; Williams, J. A. G. Time-Resolved and Two-Photon Emission Imaging Microscopy of Live Cells with Inert Platinum Complexes. *Proc. Natl. Acad. Sci. U.S.A.* **2008**, *105*, 16071−16076.
(37) Koo, C.-K.; Wong, K.-L.; Man, C. W.-L.; Lam, Y.-W.; So, L. K.-Y.; Tam, H.-L.; Tsao, S.-W.; Cheah, K.-W.; Lau, K.-C.; Yang, Y.-Y.; Chen, J.-C.; Lam, M. H.-W. Two-Photon Plasma Membrane Imaging in Live Cells by an Amphiphilic, Water-Soluble Cyctometalated Platinum(II) Complex. *Inorg. Chem.* **2009**, *48*, 7501−7503.
(38) Kondrashina, A. V.; Dmitriev, R. I.; Borisov, S. M.; Klimant, I.; O'Brien, I.; Nolan, Y. M.; Zhdanov, A. V.; Papkovsky, D. B. A Phosphorescent Nanoparticle-Based Probe for Sensing and Imaging of (Intra)Cellular Oxygen in Multiple Detection Modalities. *Adv. Funct. Mater.* **2012**, *22*, 4931−4939.
(39) Yu, M.; Zhao, Q.; Shi, L.; Li, F.; Zhou, Z.; Yang, H.; Yi, T.; Huang, C. Cationic Iridium(III) Complexes for Phosphorescence Staining in the Cytoplasm of Living Cells. *Chem. Commun.* **2008**, *44*, 2115−2117.
(40) Leung, S. K.; Liu, H. W.; Lo, K. K. W. Functionalization of Luminescent Cyclometalated Iridium(III) Polypyridine Complexes with A Fluorous Moiety: Photophysics, Protein-Binding, Bioconjugation, and Cellular Uptake Properties. *Chem. Commun.* **2011**, *47*, 10548−10550.
(41) Yan, Q.; Yue, K.; Yu, C.; Zhao, D. Oligo- and Polyfluorene-Tethered *fac*-Ir(ppy)$_3$: Substitution Effects. *Macromolecules* **2010**, *43*, 8479−9487.
(42) Yan, Q.; Fan, Y.; Zhao, D. Unusual Temperature-Dependent Photophysics of Oligofluorene-Substituted Tris-Cyclometalated Iridium Complexes. *Macromolecules* **2012**, *45*, 133−141.
(43) Wang, F.; Bazan, G. C. Aggregation-Mediated Optical Properties of pH-Responsive Anionic Conjugated Polyelectrolytes. *J. Am. Chem. Soc.* **2006**, *128*, 15786−15792.
(44) Pu, K. Y.; Fang, Z.; Liu, B. Effect of Charge Density on Energy-Transfer Properties of Cationic Conjugated Polymers. *Adv. Funct. Mater.* **2008**, *18*, 1321−1328.
(45) Liu, B.; Dishari, S. K. Synthesis, Characterization, and Application of Cationic Water-Soluble Oligofluorenes in DNA-Hybridization Detection. *Chem.—Eur. J.* **2008**, *14*, 7366−7375.
(46) Liu, S.-J.; Zhao, Q.; Fan, Q.-L.; Huang, W. A Series of Red-Light-Emitting Ionic Iridium Complexes: Structures, Excited State Properties, and Application in Electroluminescent Devices. *Eur. J. Inorg. Chem.* **2008**, 2177−2185.
(47) No DLS signal was detected from methanol solutions of **1**, **2**, or **3**, indicating that no evident intermolecular aggregation occurred under such conditions.
(48) Rao, J. P.; Geckeler, K. E. Polymer Nanoparticles: Preparation Techniques and Size-Control Parameters. *Prog. Polym. Sci.* **2011**, *36*, 887−913.
(49) Li, K.; Pu, K. Y.; Cai, L.; Liu, B. Phalloidin-Functionalized Hyperbranched Conjugated Polyelectrolyte for Filamentous Actin Imaging in Living Hela Cells. *Chem. Mater.* **2011**, *23*, 2113−2119.
(50) Pu, K. Y.; Li, K.; Shi, J.; Liu, B. Fluorescent Single-Molecular Core-Shell Nanospheres of Hyperbranched Conjugated Polyelectrolyte for Live-Cell Imaging. *Chem. Mater.* **2009**, *21*, 3816−3822.
(51) Pu, K. Y.; Li, K.; Liu, B. A Molecular Brush Approach to Enhance Quantum Yield and Suppress Nonspecific Interactions of Conjugated Polyelectrolyte for Targeted Far-Red/Near-Infrared Fluorescence Cell Imaging. *Adv. Funct. Mater.* **2010**, *20*, 2770−2777.
(52) Ye, F.; Wu, C.; Jin, Y.; Chan, Y.-H.; Zhang, X.; Chiu, D. T. Ratiometric Temperature Sensing with Semiconducting Polymer Dots. *J. Am. Chem. Soc.* **2011**, *133*, 8146−8149.
(53) Li, K.; Pan, J.; Feng, S.-S.; Wu, A. W.; Pu, K.-Y.; Liu, Y.; Liu, B. Generic Strategy of Preparing Fluorescent Conjugated-Polymer-Loaded Poly(DL-Lactide-co-Glycolide) Nanoparticles for Targeted Cell Imaging. *Adv. Funct. Mater.* **2009**, *19*, 3535−3542.
(54) Medley, C. D.; Bamrungsap, S.; Tan, W.; Smith, J. E. Aptamer-Conjugated Nanoparticles for Cancer Cell Detection. *Anal. Chem.* **2011**, *83*, 727−734.
(55) Liu, B.; Gaylord, S. S.; Wang, S.; Bazan, G. C. Effect of Chromophore-Charge Distance on the Energy Transfer Properties of Water-Soluble Conjugated Oligomers. *J. Am. Chem. Soc.* **2003**, *125*, 6705−6714.
(56) Ryan, S. M.; Mantovani, G.; Wang, X.; Haddleton, D. M.; Brayden, D. J. Advances in PEGylation of Important Biotech Molecules: Delivery Aspects. *Expert Opin. Drug Delivery* **2008**, *5*, 371−383.
(57) The time-resolved emissions of **NP2** in water and cells slightly deviated from monoexponential functions (Figure S11), and the fitting was not improved when higher-order exponential functions were applied. This might reflect inhomogeneity inside the nanoparticles.
(58) Zhang, K. Y.; Li, S. P.-Y.; Zhu, N.; Or, I. W.-S.; Cheung, M. S.-H.; Lam, Y. W.; Lo, K. K.-W. Structure, Photophysical and Electrochemical Properties, Biomolecular Interactions, and Intracellular Uptake of Luminescent Cyclometalated Iridium(III) Dipyridoquinoxaline Complexes. *Inorg. Chem.* **2010**, *49*, 2530−2540.
(59) Belfield, K. D.; Bondar, M. V.; Przhonska, O. V.; Schafer, K. J. Photochemical Properties of (7-Benzothiazol-2-yl-9,9-didecylfluoren-2-yl)diphenylamine under One- and Two-Photon Excitation. *J. Photochem. Photobiol. A: Chem.* **2004**, *162*, 569−574.
(60) Namely, the wavelength of 800 nm was in the overlapped region of 2PA and 3PA spectra of **NP2**. By taking advantage of the different dependences of 2PA and 3PA on the excitation power density, applying significantly varied incident-light power to measure the 2PA and 3PA cross-sections is an established procedure for molecules having overlapped 2PA and 3PA spectra. For a related example, see: Morisue, M.; Ogawa, K.; Kamada, K.; Ohta, K.; Kobuke, Y. Strong Two-Photon and Three-Photon Absorptions in the Antiparallel Dimer

of a Porphyrin−Phthalocyanine Tandem. *Chem. Commun.* **2010**, *46*, 2121−2123.
(61) Hernández, F. E.; Belfield, K. D.; Cohanoschi, I. Three-Photon Absorption Enhancement in a Symmetrical Charge Transfer Fluorene Derivative. *Chem. Phys. Lett.* **2004**, *391*, 22−26.
(62) Cohanoschi, I.; García, M.; Toro, C.; Belfield, K. D.; Hernández, F. E. Three-Photon Absorption of a New Series of Halogenated Fluorene Derivatives. *Chem. Phys. Lett.* **2006**, *430*, 133−138.
(63) Law, G.-L.; Wong, K.-L.; Man, C. W.-Y.; Wong, W.-T.; Tsao, S.-W.; Lam, M. H.-W.; Lam, P. K.-S. Emissive Terbium Probe for Multiphoton in Vitro Cell Imaging. *J. Am. Chem. Soc.* **2008**, *130*, 3714−3715.
(64) Eliseeva, S. V.; Auböck, G.; Mourik, F.; Cannizzo, A.; Song, B.; Deiters, E.; Chauvin, A.-S.; Chergui, M.; Bünzli, J.-C. G. Multiphoton-Excited Luminescent Lanthanide Bioprobes: Two- and Three-Photon Cross Sections of Dipicolinate Derivatives and Binuclear Helicates. *J. Phys. Chem. B* **2010**, *114*, 2932−2937.
(65) Massue, J.; Olesiak-Banska, J.; Jeanneau, E.; Aronica, C.; Matczyszyn, K.; Samoc, M.; Monnereau, C.; Andraud, C. Remarkable Effect of Iridium Cyclometalation on the Nonlinear Absorption Properties of a Quadrupolar Imine Ligand. *Inorg. Chem.* **2013**, *59*, 10705−10707.
(66) Feng, X.; Lv, F.; Liu, L.; Tang, H.; Xing, C.; Yang, Q.; Wang, S. Conjugated Polymer Nanoparticles for Drug Delivery and Imaging. *ACS Appl. Mater. Interfaces* **2010**, *2*, 2429−2435.
(67) Pu, K.-Y.; Shi, J.; Cai, L.; Li, K.; Liu, B. Affibody-Attached Hyperbranched Conjugated Polyelectrolyte for Targeted Fluorescence Imaging of HER2-Positive Cancer Cell. *Biomacromolecules* **2011**, *12*, 2966−2974.